



Flexible Harmonic Current Compensation Strategy Applied in Single and Three-Phase Photovoltaic Inverters

A. F. Cupertino, G. L. E. Mata, H. A. Pereira and L. S.Xavier.

Published in:

International Journal of Electrical Power & Energy Systems

DOI (*link to publication from Publisher*):

[10.1016/j.ijepes.2018.07.017](https://doi.org/10.1016/j.ijepes.2018.07.017)

Publication year:

2019

Document Version:

Accepted author manuscript, peer reviewed version

Citation for published version:

A. F. Cupertino, G. L. E. Mata, H. A. Pereira, L. S. Xavier, " Flexible Harmonic Current Compensation Strategy Applied in Single and Three-Phase Photovoltaic Inverters ," International Journal of Electrical Power & Energy Systems, vol. 104, pp. 358-369, January 2019.

doi: 10.1016/j.ijepes.2018.07.017

General rights

Copyright and moral rights for the publications made accessible in the public portal are retained by the authors and/or other copyright owners and it is a condition of accessing publications that users recognise and abide by the legal requirements associated with these rights.

- Users may download and print one copy of any publication from the public portal for the purpose of private study or research.
- You may not further distribute the material or use it for any profit-making activity or commercial gain
- You may freely distribute the URL identifying the publication in the public portal

Take down policy

If you believe that this document breaches copyright please contact us at geseufv@gmail.com providing details, and we will remove access to the work immediately and investigate your claim.

Flexible Harmonic Current Compensation Strategy Applied in Single and Three-Phase Photovoltaic Inverters

Heverton A. Pereira^a, Guilherme L. E. da Mata^a, Lucas S. Xavier^c, Allan F. Cupertino^{b,c}

^a*Department of Electrical Engineering, Federal University of Viçosa, Av. P. H. Rolfs, s/n, 36570-000, Viçosa - MG, Brazil*

^b*Department of Materials Engineering, Federal Center for Technological Education of Minas Gerais, Av. Amazonas, 5253, 30421-169, Belo Horizonte - MG, Brazil*

^c*Graduate Program in Electrical Engineering - Universidade Federal de Minas Gerais - Av. Antônio Carlos 6627, 31270-901, Belo Horizonte, MG, Brazil*

Abstract

Non-linear loads connected to power system have increased considerably in the recent decades. Traditional generation based on hydro and thermal power plants cannot mitigate harmonic currents. However, due to the increased connection of photovoltaic into the power system, its power electronic converter can be used to perform ancillary services such as harmonic current compensation. This work presents a dynamic method based on the Second Order Generalized Integrator coupled with a phase locked loop structure to detect and compensate the most predominant harmonic current components from the power system. It is also presented an extension to detect multiple harmonics, according to the amplitude. Technical issues related with the harmonic current compensation strategy, and its implementation for both single and three-phase PV inverters are explored to demonstrate the functionality and efficiency of the method. The results show the harmonic current compensation being compensated by a PV inverter. Finally, a losses analysis were performed in the LCL filter. The magnetic and damping resistor losses are more impacted due to high harmonic

Email addresses: heverton.pereira@ufv.br (Heverton A. Pereira), glevangelista48@gmail.com (Guilherme L. E. da Mata), lucas.xavier@ufv.br (Lucas S. Xavier), afcupertino@ieee.org (Allan F. Cupertino)

current compensation.

Keywords: Ancillary Services, Harmonic Current Detection Method,
Harmonic Current Compensation, Single and Three-phase PV inverters

1. Introduction

The classic infrastructure of electrical power systems consists on large scale centralized generation, distributed over long transmission lines [1]. Nowadays, distributed generation (DG) systems have changed this traditional conception. DG systems are receiving more attention whereas environmental concerns and energy demand grow over the world [2]. Furthermore, DG systems may be installed inside consumer units, which reduces losses over distribution and transmission systems [3]. Such benefits brought huge development in renewable energy sources in recent years, especially photovoltaic (PV) energy, whose cost was reduced in 75% in less than 10 years [4].

Compared with hydro and thermal power plants, PV systems have electronic converters that inject high order harmonic current components into the power system. [3, 5]. These high order harmonic component can be minimized using passive filters. On the order hand, the growing presence of nonlinear loads, generally, injecting low order harmonic current components, can reduce the distribution system power quality [6].

Since solar irradiance varies during the day, inverters usually work below their nominal operation point [7], as illustrated in Figure 1. Thus, whenever the inverter current does not exceed its nominal value, it can be used to improve the power quality [8, 9]. Ancillary services, such as reactive power compensation [10, 11], reactive injection during faults [12], voltage and frequency regulation [12] and harmonic current compensation [6, 10] are some of the contributions that PV inverters can aggregate to improve the power system stability.

Current total harmonic distortion (THD) level is an important index in power systems harmonic analysis. Some standards define that the current THD level must be below 5% [13, 14]. Some methods to reduce the grid harmonic

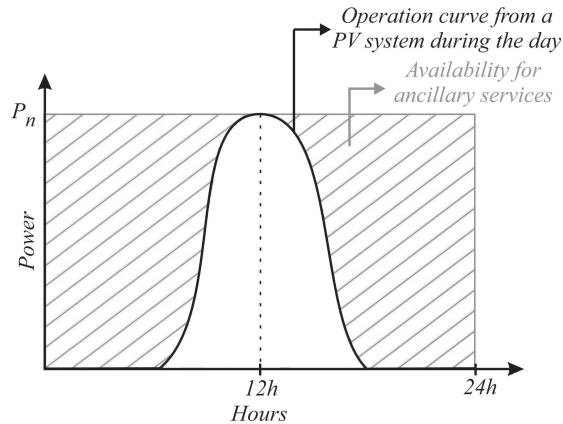


Figure 1: Power generated by a PV system during a sunny day.

current distortions can be found in literature. The most conventional ones use passive [15] and active [16, 17] filters, or associations of both to decrease the THD level. However, once the PV plant is already installed, the use of the inverter in multifunctional operation is an economic alternative more viable than passive or active filters [18].

The detection method is an important issue to compensate harmonic current components. Some of the methods commonly found in literature realize the harmonic current detection through second order generalized integrators (SOGI) [1], instantaneous power theory [11, 17], conservative power theory [3, 7, 18], Fourier transform [19] and delayed signal cancellation [20]. Nevertheless, most of these strategies detect the whole harmonic content from the load, increasing the controller tuning complexity.

The kind of controller affects both precision and control complexity. Proportional integral (PI) controllers are easier to implement, however, it presents steady state errors, due to their limited bandwidth. This results in a lower tracking capacity and consequently loss of precision. On the other hand, proportional resonant (PR) controllers are more accurate [21], even though the need of one PR tuned in each frequency to be compensated, increasing the control complexity. An alternative to obtain low complexity and precise control is

making the controller adaptive to the harmonic components. Thus, it can follow the harmonic load variations [22].

In this work, for both single-phase and three-phase systems, a harmonic current detection is proposed through a cascade association of a SOGI and a synchronous reference frame phase-locked loop (SRF-PLL) structure. This
50 a synchronous reference frame phase-locked loop (SRF-PLL) structure. This detection structure proposed in [23] was used to synchronize the converter with the grid voltage phase angle. We have extended this concept to detect harmonic current components. Furthermore, this work shows the SRF-PLL flexibility when n -stages are cascaded. Finally, the load harmonic current components of
55 higher amplitude are compensated with a PV inverter.

Therefore, the present work provides the following contributions:

- a flexible harmonic current detection strategy based on n -stage SOGI-PLL structure with negative feedback;
- proposal of a fast algorithm to select the highest harmonic current components;
- losses in the LCL filter are computed to show the impact of the harmonic
60 current compensation in the copper and magnetic losses.

This paper is structured as follows: Section 2 describes the main parts of the PV system, including the control strategies used in both single-phase and three-phase systems. Section 3 describes the harmonic detection topology and
65 its extension for multiple harmonic components detection. Section 4 presents the case studies for both single and three-phase systems. In Section 5, the proposed harmonic detection method is verified through simulation results. Finally, the conclusions are stated in Section 6.

2. Grid Connected PV System

70 In this work, two PV systems are analyzed: a single-phase and a three-phase. Figure 2 presents a general connection scheme between the PV plant and the power system.

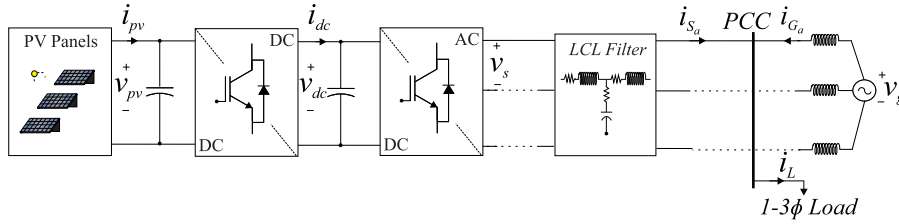


Figure 2: Grid-connected PV system.

2.1. Photovoltaic Panel, Maximum Power Point Tracking and LCL Filter

Based on the photovoltaic effect, the PV panel transforms sunlight energy into electricity. A mathematical model proposed by [24] is used to simulate a photovoltaic panel. Furthermore, the Maximum Power Point Tracking (MPPT) algorithm is extremely important for the PV system control efficiency. The Incremental Conductance (IC) method is able to extract more power than the Perturb and Observe (P&O) method [25], and it is used in this work.

The LCL filter is the structure most used to attenuate harmonics generated by the inverter switching [26]. Although LCL filter is a simple passive structure, its design requires special attention. The capacitor value is limited by the power factor at rated power (generally less than 5% of the inverter nominal power) [26]. A resistor is connected in series with the capacitor in order to reduce the resonant peak [27]. The resonant frequency should be in a range between ten times the line frequency and one-half of the switching frequency, to avoid resonance problems in the lower and upper parts of the harmonic spectrum [26]. Besides, passive damping must be sufficient to avoid oscillation, however, losses should reduce slightly the converter efficiency [27].

The losses in LCL filter can be classified in the following groups: capacitor losses, damping losses and inductor losses. LCL filters employ film capacitors with a very low series resistance and thereby negligible losses [28]. Therefore, only damping and inductor losses are considered in this work. In order to evaluate inductor losses, its physical design needs to be accomplished. The design methodology employed is based on [29].

The inductor copper losses is calculated as function of the rms current I_r :

$$P_{cp} = R_L I_r^2, \quad (1)$$

where R_L is the inductor resistance. As observed, the skin and distribution effects are not considered in this work. Finally, the magnetic losses are estimated by the improved generalized Steinmetz equation method (iGSE) [30], given by:

$$P_m = \frac{V_c}{T} \int_0^T k_i \left| \frac{dB}{dt} \right| (\Delta B)^{\beta-\alpha} dt, \quad (2)$$

$$k_i = \frac{K}{(2\pi)^{\alpha-1} \int_0^{2\pi} |\cos\theta|^\alpha 2^{\beta-\alpha}}, \quad (3)$$

100 where V_c is the magnetic core volume and K , α and β are the Steinmetz parameters, which are provided in the datasheets [29]. As observed, the flux density waveform must be known, thus the magnetic losses can be computed. $B(t)$ can be obtained from the voltage at the inductor terminals $v_L(t)$, as follows:

$$B(t) = \frac{1}{NA_c} \int v_L(t) dt. \quad (4)$$

where A_c is the cross sectional area of the inductor core.

105 2.2. Control Strategies

The PV inverter control strategies have two forms, the dc/dc stage, with boost converter, and the dc/ac stage, with the inverter.

2.2.1. Dc/dc stage

The dc/dc stage converter is commonly used for booster the input voltage
 110 level of the inverter, ensuring the acceptable voltage level for startup and extending its operation range during low irradiance conditions. In single-phase system, the use of dc/dc is even more important due to power oscillation in the 2nd harmonic frequency. This power oscillation results in dc-link voltage fluctuation and reduces the MPPT efficiency, when the PV modules are connected directly
 115 to the dc-link. For this reason, it is advisable to perform MPPT algorithm in

dc/dc stage control for single-phase applications. The boost converter is widely used for these cited purposes [31].

The connection of the PV array to the boost converter is shown in Fig. 3. The PV array model is linearized around the nominal maximum power point, since the operation of the device should occur preferably around this point. Therefore, the PV array can be represented by a linear circuit composed by an equivalent voltage source (v_{mpp}) and corresponding resistance (R_{mpp}) at MPP. The dc-link can be represented by a voltage source (v_{dc}), assuming that the voltage is already controlled. The average values of the capacitor voltage (v_{pv}) and inductor current (i_{Lb}) over one switching period can be obtained by:

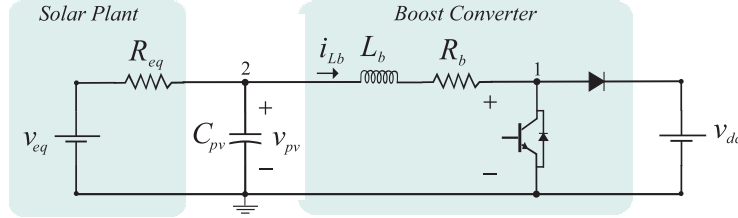


Figure 3: Boost converter connected to linearized solar modules model.

$$C_{pv} \frac{d\langle v_{pv} \rangle}{dt} = \frac{v_{eq}}{R_{eq}} - \frac{\langle v_{pv} \rangle}{R_{eq}} - \langle i_{Lb} \rangle, \quad (5)$$

$$L_b \frac{d\langle i_{Lb} \rangle}{dt} = \langle i_L \rangle R_b + (1-d)v_{dc} - \langle v_{pv} \rangle, \quad (6)$$

where L_b is the boost converter inductance, R_b is the inductor equivalent series resistance and d is duty cycle. A small-signal model is adopted to linearize the converter model [32], given by:

$$G_{vi}(s) = \frac{\hat{v}_{pv}}{\hat{i}_{Lb}} = -\frac{1}{sC_{pv} + \frac{1}{R_{eq}}}, \quad (7)$$

$$G_{id}(s) = \frac{\hat{i}_{Lb}}{\hat{d}} = \frac{v_{dc}}{sL_b + R_b}, \quad (8)$$

where “ $\hat{}$ ” means small signal term.

stage dynamics in $\alpha\beta$ coordinates is given by:

$$v_{s,\alpha} - Ri_{s,\alpha} - L\frac{di_{s,\alpha}}{dt} - v_{g,\alpha} = 0, \quad (10)$$

$$v_{s,\beta} - Ri_{s,\beta} - L\frac{di_{s,\beta}}{dt} - v_{g,\beta} = 0, \quad (11)$$

where $L = L_f + L_g$ and $R = R_f + R_g$ is the equivalent series resistance of the filter, $v_{s,\alpha}$ and $v_{s,\beta}$ are the voltages synthesized at the inverter terminals, $v_{g,\alpha}$ and $v_{g,\beta}$ are the voltages at the (PCC), $i_{s,\alpha}$ and $i_{s,\beta}$ are the currents from the inverter in stationary ($\alpha - \beta$) reference frame.

The outer loop control computes the active power injected by the inverter on the grid (p_{inv}). For this case study, zero reactive power (\bar{q}) is injected by the PV inverter into the grid. By using (12), it is possible to obtain the $\alpha\beta$ components from the injected fundamental current.

$$\begin{bmatrix} i_{s\alpha} \\ i_{s\beta} \end{bmatrix} = \frac{A}{v_{g\alpha}^2 + v_{g\beta}^2} \begin{bmatrix} v_{g\alpha} & v_{g\beta} \\ v_{g\beta} & -v_{g\alpha} \end{bmatrix} \begin{bmatrix} p_{inv} \\ \bar{q}^* \end{bmatrix} \quad (12)$$

where $A = 1$ for three-phase system and $A = 2$ for single-phase system. It is important to point out that only the α -component is controlled in single-phase system.

The currents given by (12) are added to the detected harmonic current components which results in the reference signal. For the inverter current control loop, it is performed by means of proportional multi-resonant controllers (PMR) adjusted dynamically at each harmonic frequency to be compensated. The PMR transfer function can be represented by [33]:

$$G_C(s) = K_p^r + \sum_{h=1}^n K_{i,h}^r \overbrace{\frac{s}{s^2 + \omega_h^2}}^{R_h(s)}, \quad (13)$$

where K_p^r is the proportional gain, h is the harmonic order ($h = 1, 2, 3, \dots, n$), ω_h are resonant frequencies, and $K_{i,h}^r$ are the resonant gains for each harmonic frequency.

3. Harmonic Current Detector Based on SOGI-PLL

In this section, the single-phase representation of the harmonic current detection method is addressed. This current detector structure is shown in Figure 6(a).

165 It is based on a cascaded SOGI-PLL structure [22, 23] as represented in Figure 6(b). This method takes advantage of the interaction between the SOGI adaptive filter, whose bandwidth depends only on the gain k [23].

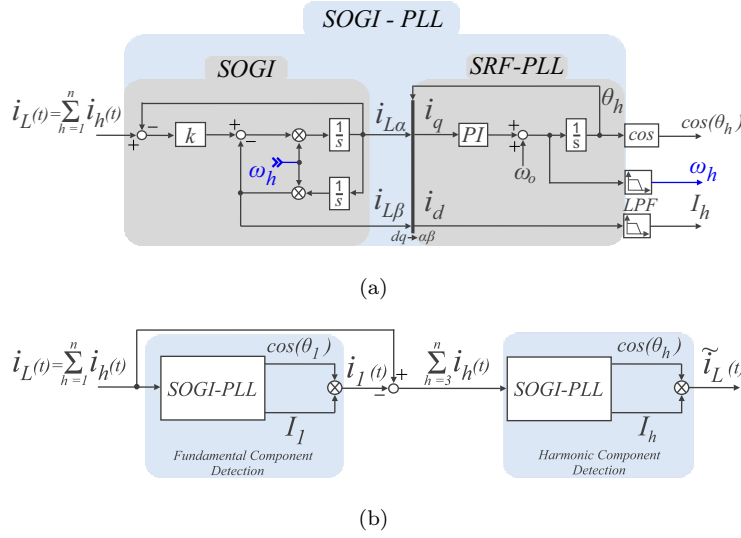


Figure 6: (a) General structure of SOGI-PLL. (b) Current harmonic detection method based on SOGI-PLL.

The input current $i_L(t)$, as shown in Fig. 6, is a signal composed of all frequency components from the load current. The first stage aims to detect the load fundamental current component $i_1(t)$. The SOGI-PLL structure of this stage extracts the amplitude I_1 , frequency ω_1 and phase angle θ_1 information of the fundamental component. A low-pass filters (LPF) in the amplitude and frequency detection are important to avoid the effect of the harmonic components that the SOGI-PLL bandwidth cannot suppress. This signal is reconstructed, represented by $i_1(t)$, and subtracted from the input current.

The next stage of the harmonic component detection extracts the amplitude, frequency and phase angle information from the predominant harmonic component

presented in the load current. The current signal $\tilde{i}_L(t)$ is reconstructed and sent to the control loop to perform the harmonic compensation of this predominant load harmonic current.

The frequency of the detected harmonic is used as feedback to tune the resonant controller. In this case, only two resonant controllers are needed, the first one for controlling the fundamental current and the second, dynamically controlling the predominant harmonic of the load current [22].

3.1. Multi-Harmonic Current Detector

The structure shown in Figure 6(b) can be extended to detect any number of harmonic current components in the load current, as shown in Figure 7. In this structure, n SOGI-PLLs can be connected in cascade. In this work, the strategy of negative feedback is included in the harmonic detector based on SOGI-PLL. This concept consists of subtracting the detected harmonic components from the input signals of the previous stages, as shown in Figure 7. For example, in the first stage, where the current fundamental component is detected, all harmonic currents detected by the following stages are removed from the input current $i_L(t)$. Thereby, in steady state, a cleaner signal is provided for each detector stage, which reduces the effects of the SOGI-PLL bandwidth on the detected signal.

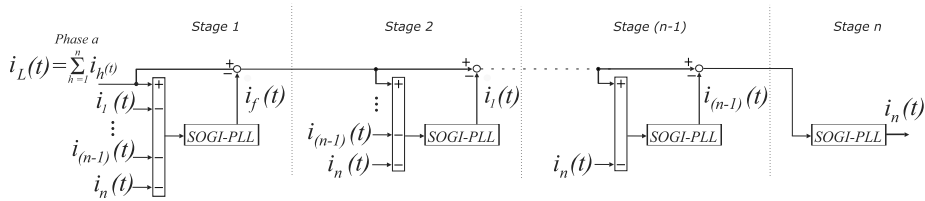


Figure 7: Multi Stage Harmonic Detector.

Together with the harmonic detector, it is used an algorithm to select the harmonic components of higher amplitudes for compensation. For example, if there are three implemented detector stages, there are only two resonant controllers. Thus, the proposed algorithm sends only the two highest harmonic

components to be compensated, and adaptively the two resonant controllers are tuned. The flowchart of this algorithm is shown in Figure 8. Basically, this algorithm compares the amplitudes of the detected signals and sends the two highest harmonic signals to the current control loop. The phase signal is used
 205 in the algorithm for harmonic current component reconstruction.

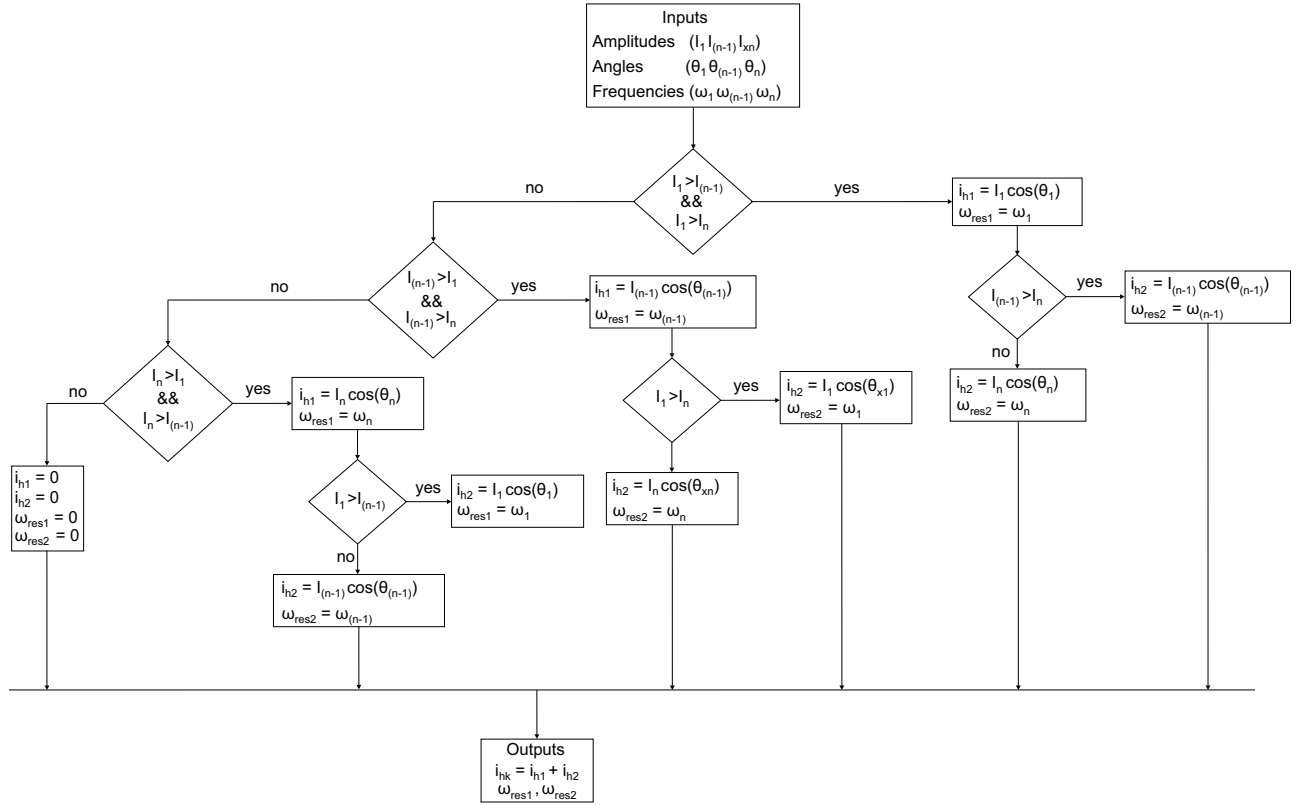


Figure 8: The algorithm flowchart to select the two highest harmonic components for compensation in single-phase system

3.2. Multi-Harmonic Current Detector for Three-Phase System

The harmonic current detector can be applied in balanced three-phase systems in order to perform the harmonic compensation selectively. Similarly to the single-phase version, showed in Figure 7, the first stage detects the load current
 210 fundamental component $i_1(t)$ of the phase a . This fundamental component is

subtracted from the load current. The resultant signal contains load current harmonic components, which are detected in the next stages.

The difference in the harmonic current detector between the three-phase system and single-phase system is how the signal is reconstructed in the algorithm
 215 to select the harmonic components of higher amplitudes for compensation, shown in Figure 8. Considering a balanced three-phase system, the detected phases of each harmonic are displaced by $2\pi h_x/3$ radians, where h_x is the harmonic order detected in each stage. Thereby, the signal is reconstructed for the three phases, considering the displacements of 120° between them. The
 220 current reference in abc coordinate is found through the sum of each harmonic term. Finally, the $\alpha\beta$ currents are obtained and sent to the inverter control.

4. Case Study

The systems described in this work were simulated using the software PLECS and Matlab environment. In the single-phase case study, the PV array is
 225 composed of 2 strings with 10 panels of 250 W connected in series, resulting in a system of 5 kW. In the three-phase case study, the PV array is composed of 1 string with 20 panels of 250 W in series. The PV panel used in this work has the characteristics presented in Table 1.

Table 1: PV Panel specification for standard conditions (1000 W/m^2 and 25°C).

Parameters	Value
Nominal Power	250 W
Short Circuit Nominal Current	$I_{scn} = 8.5 \text{ A}$
Open Circuit Nominal Voltage	$V_{ocn} = 35.5 \text{ V}$
Maximum Power Point Current	$I_{mp} = 7.99 \text{ A}$
Maximum Power Point Voltage	$V_{mp} = 31.29 \text{ V}$

The load used in the single-phase case study is composed by a linear load
 230 that consumes 5 kW and a non-linear load composed by three harmonic currents of 3^{rd} , 5^{th} and 7^{th} orders, with amplitudes 10 A, 6 A and 3 A, respectively.

At 4 seconds of simulation, the non-linear load changes its composition into harmonic currents of 3^{rd} , 5^{th} and 7^{th} orders, with amplitudes of 3 A, 10 A and 6 A, respectively, as shown in Figure 9.

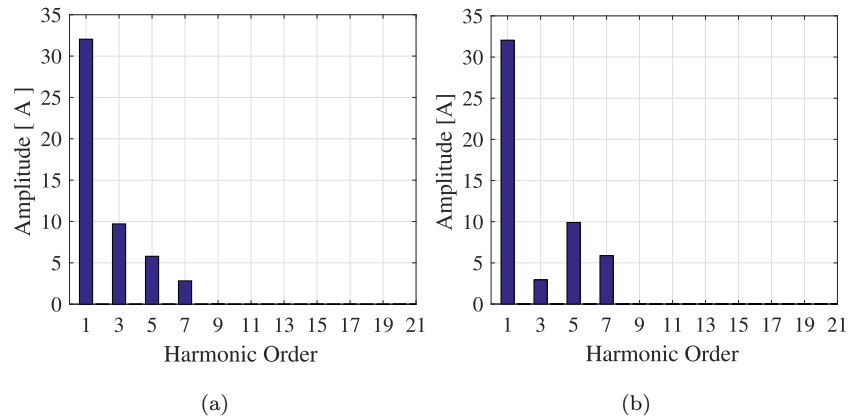


Figure 9: Composition of the non-linear load in single-phase simulation: (a) load profile before $t = 4s$. (b) load profile after $t = 4s$.

235 The load used in the three-phase case study is also composed of a linear load of 5 kW and a non-linear load composed of 5^{th} , 7^{th} and 11^{th} orders, with amplitudes of 10 A, 6 A and 3 A, respectively. At 4 seconds, these amplitudes change to 3 A, 10 A and 6 A, respectively, as shown in Figure 10.

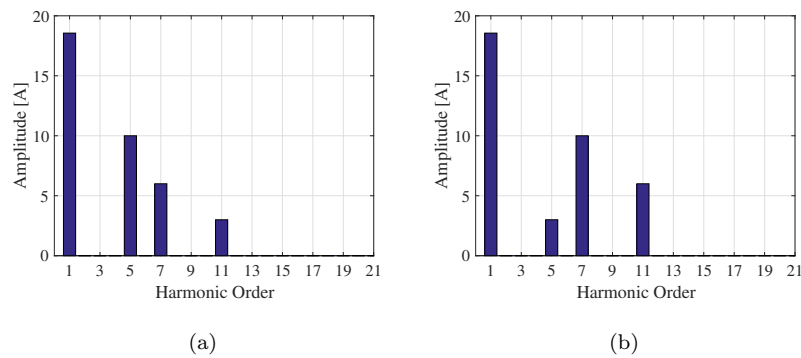


Figure 10: Composition of the non-linear load in three-phase simulation: (a) load profile before $t = 4s$. (b) load profile after $t = 4s$.

The physical design of the LCL filter inductors follows the methodology
 240 proposed in [29]. The parameters of the inductors of single and three phase
 inverters are shown in Table 2.

Table 2: Physical parameters of the LCL filter inductors

Single-Phase System	Value
Core part number	58337
Number of turns	130
Cross sectional area	678 mm^2
Core volume	220000 mm^3
Three-Phase System	Value
Core part number	58737
Number of turns	80
Cross sectional area	497 mm^2
Core volume	91400 mm^3

The harmonic detector parameters are shown in Table 3, and the single and
 three-phase inverter parameters can be found in Tables 4 and 5, respectively.
 The solar irradiance is maintained at 500 W/m^2 . In both case studies, four
 245 stages of the harmonic current detector are employed. However, only the two
 most predominant harmonic components of the load current are compensated.
 In this case, three PR controllers were used: one was adjusted to the fundamental
 frequency of the grid, and the other two were tuned on the frequency of the two
 harmonic components with higher amplitude.

Table 3: Harmonic Detector Parameters

Structure	Value
SOGI-PLL Parameters of the 1st Stage	$k_{SOGI} = 0.8$
	$\xi = 0.707$
	$\omega_n = 6\pi$
SOGI-PLL Parameters of the 2nd, 3rd, 4th Stages	$k_{SOGI} = 0.8$
	$\xi = 0.707$
	$\omega_n = 60\pi$

Table 4: Single Phase Simulation Parameters

System Parameters	Value
Switching frequency	12 <i>kHz</i>
Sampling Frequency	12 <i>kHz</i>
LCL Filter Inductors	1 <i>mH</i> / 40 <i>mΩ</i>
LCL Filter Capacitor	3.8 μF
LCL Filter Damping Resistance	4 Ω
PCC Voltage	220 <i>V_{rms}</i>
Dc Link Voltage	390 <i>V</i>
Dc Bus Capacitor	500 μF
Controllers Gains	Value
Dc-link Controller	$K_{p-sdc} = 0.145$
	$K_{i-sdc} = 1.244$
Boost Controller	$K_{p-VM} = 1.508$
	$K_{i-VM} = 158.733$
	$K_{p-IM} = 0.193$
	$K_{i-IM} = 0.387$
Resonant Controller	$K_{p-res} = 14.833$
	$K_{i-res} = 2000$

Table 5: Three Phase Simulation Parameters

System Parameters	VALUE
Switching frequency	12 <i>kHz</i>
Sampling frequency	12 <i>kHz</i>
LCL filter inductors	1 <i>mH</i> / 31.2 <i>mΩ</i>
LCL filter capacitor	3.37 μF
LCL filter damping resistance	4 Ω
PCC voltage	220 <i>V_{rms}</i>
Dc-link capacitor	1000 μF
Controllers Gains	VALUE
Dc-link controller	$K_{p-sdc} = 0.0345$
	$K_{i-sdc} = 0.197$
Resonant controller	$K_{p-res} = 14.833$
	$K_{i-res} = 2000$

250 **5. Simulation and Results**

5.1. *Single-phase system*

Figure 11(a) shows the voltage control of the PV panels. This voltage follows the maximum power point voltage detected by the MPPT algorithm. Figure 11(b) shows the inverter dc-link voltage control. This voltage is controlled, with some oscillations observed only in the beginning of the harmonic compensation and at the change of the non-linear load. Figure 11(c) shows the boost inductor current control.

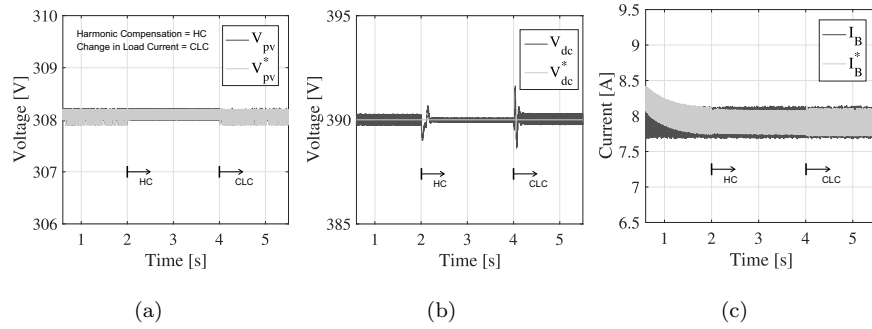


Figure 11: (a) PV panels voltage control. (b) Inverter dc-link voltage control. (c) Boost current control

The harmonic current detection starts at 1.5 seconds of simulation in the first SOGI-PLL structure, with 0.3 seconds between the initialization of each, and the harmonic compensation (HC) at 2 seconds. This procedure aims to allow initial detection stabilization before the compensation starts. The two harmonic signals with higher amplitude are compensated in the current control loop. The third one is used only in the detector feedback, thus, improving precision in the amplitude detection.

Figure 12 shows the detected current amplitudes and frequencies. The detected current compensation can be observed in Figures 13 and 14. Figure 13 shows the inverter harmonic current components and Figure 14 shows the grid harmonic current components. There is no compensation before $t = 1s$, and

the grid current presents all the harmonic components from the load. The grid current THD at this time is 75 %, as shown in Table 6. Compensation occurs at $t = 2s$. The 3rd and 5th harmonics are compensated and these components appear in the inverter current. The grid current THD at this time is 17 %. In $t = 4s$, the non-linear load composition changes and the 5th and 7th harmonics are compensated. After 4 seconds, the grid current THD is 19 %.

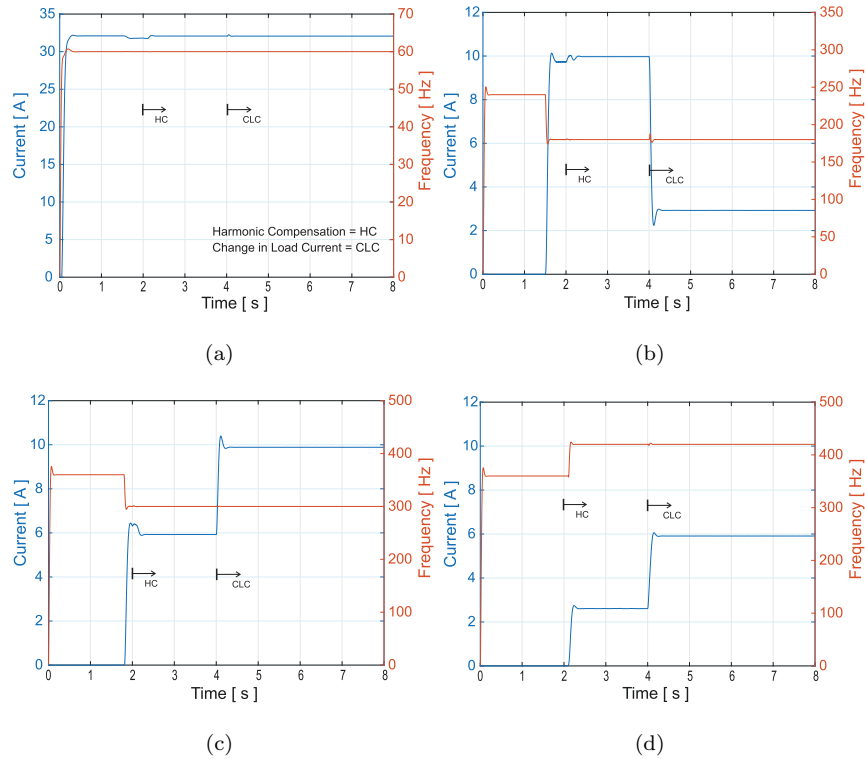


Figure 12: (a) Load fundamental component detection. (b) Load highest amplitude harmonic component detection. (c) Load 2nd highest amplitude harmonic component detection. (d) Load 3rd highest amplitude component detection.

Once harmonic current compensation is an ancillary service executed by the inverter, an important issue to be verified is the losses in the LCL filter, including core losses and copper losses. Once, the inverter filter is composed of inductors and capacitors, the filter impedance changes with different harmonic

Table 6: Grid current THD in the single-phase case study

Simulation Time (seconds)	Grid Current THD
$t < 2$	75 %
$2 \leq t < 4$	17 %
$t \geq 4$	19 %

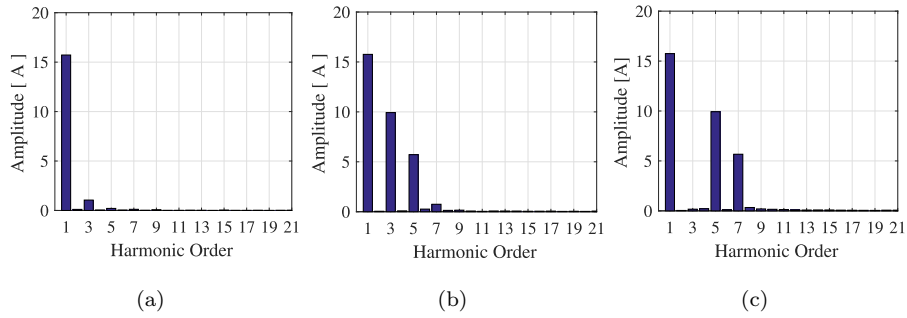


Figure 13: Inverter current spectra (a) without HC compensation, $t < 1s$, (b) compensating the first load profile, $2 < t < 4s$ (c) compensating the second load profile, $t > 4s$.

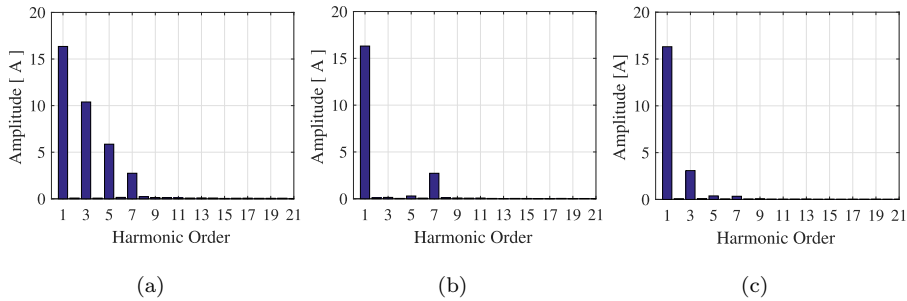


Figure 14: Grid current spectra (a) without HC compensation $t < 1s$, (b) compensating the first load profile $2 < t < 4s$ and (c) compensating the second load profile $t > 4s$.

components, and the losses in the capacitor tends to grow as the harmonic order increases.

To illustrate this fact, it is made a study to verify the filter core and cooper losses for four harmonic current components and the fundamental component (1st component), considering five different amplitude values. The system compensates

the 5th, 7th, 11th and 13th harmonic current components, each one with amplitude
 285 varying of 0.2 pu, 0.4 pu, 0.6 pu, 0.8 pu and 1 pu. The results obtained are shown
 in Figure 15. This figure shows the LCL filter losses when the PV system injects
 only the fundamental current component (active power) and only compensating
 one harmonic current component. It is important to note that only one harmonic
 order is injected at a time.

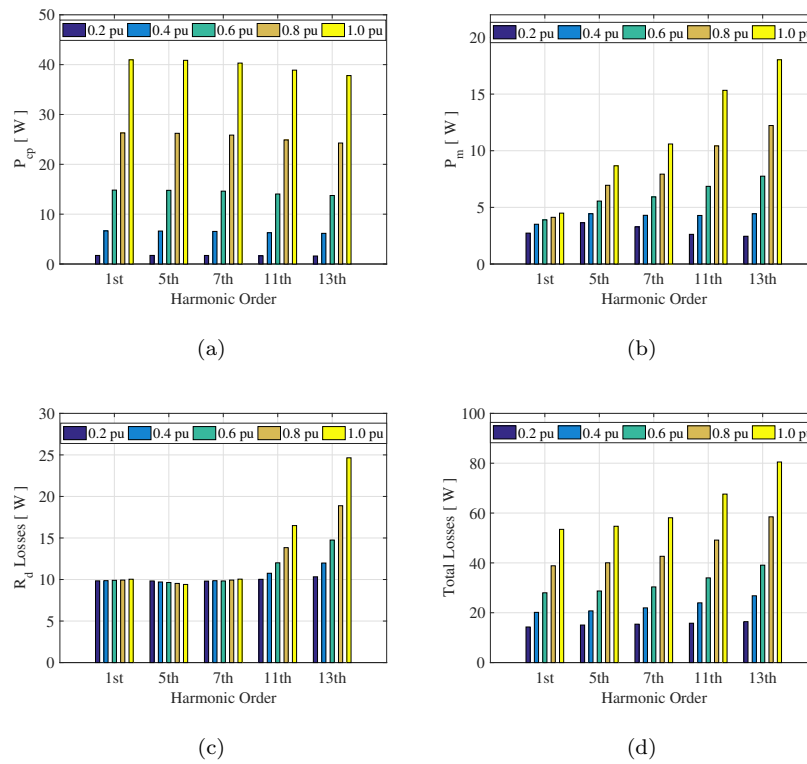


Figure 15: Losses in the single-phase LCL filter during harmonic compensation (a) Total copper losses (b) Total core losses (c) Damping resistor losses (e) Total LCL filter losses.

290 Figure 15(a) shows the total filter copper losses. It is possible to note
 that, for each harmonic order, the power losses increase with the RMS current.
 However, when harmonic order increases, it can be observed a small difference
 between power losses for the same conditions since the RMS value of the grid

side inductor current (controlled quantity) related to the compensated harmonic
295 current is the same. Instead the grid side inductor current, the RMS value of
the converter side inductor current changes with harmonic order, for the same
amplitude. This can be explained due to the fact that the capacitor current
magnitudes depend on the frequency. Nevertheless, disregarding the presence
of voltage harmonics in the grid, it can be concluded that the capacitor current
300 leads the compensated current by 180 degrees. For this reason, the ohmic losses
in the internal inductor of the LCL filter decrease and as a global result, the
ohmic losses have a slight reduction when the harmonic order increases. The
contribution of the skin effect is disregarded in this analysis.

Figure 15(b) shows the total filter core losses. The core losses in the converter
305 side inductor are greater than in the grid side inductor due to the higher
harmonic current content. The core losses depend on the compensated harmonic
current and on the switching harmonic current components. During low current
amplitudes, the switching content dominates and the losses do not vary so much
with the harmonic order. For large compensated harmonic current amplitudes,
310 the contribution of this current component in the core losses is more significant,
increasing considerably with the harmonic order. Furthermore, the flux density
in the inductor core increases with the current and consequently the magnetic
loss increases. This can be observed for all harmonic orders

Figure 15(c) shows the damping resistor losses. It is possible to note that the
315 losses increase with the harmonic order frequency, since the capacitor current
increases. The damping resistor losses are dependent on the compensated
harmonic current and on the harmonic currents generated by the converter
switching. For harmonic current components until the 7th order, the losses
associated to the switching frequency is predominant and the variation of losses
320 become dependent of this component. For harmonic current components with
higher frequency, the compensated harmonic current component becomes dominant
in the capacitor current. Thus, losses in the capacitor tend to increase with the
amplitude of the compensated harmonic component.

Finally, Figure 15(d) shows the total losses in the LCL filter. Note that the

325 losses increase with the harmonic order and current amplitude. When the PV
 system injects only active power, the total power losses are 54 W for 1 pu. Note
 that, when the PV inverter only injects 1 pu of 13th harmonic current the total
 power losses are 80 W, approximately.

5.2. Three-Phase System

330 The voltage dynamic of the inverter dc-link is illustrated in Figure 16. The
 voltage reference v_{dc}^* is calculated by the MPPT algorithm. Harmonic current
 detection starts at 1.5 seconds and the harmonic current compensation, at 2
 seconds.

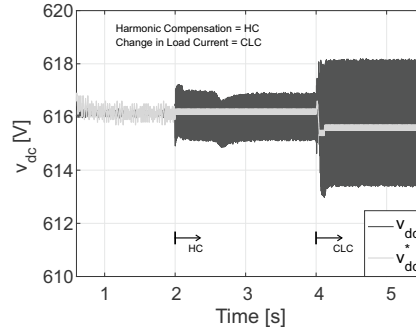


Figure 16: Inverter dc-link voltage control.

The detected current amplitudes and frequencies are shown in Figure 17.
 335 The SOGI-PLLs are initialized at different times, with 0.3 seconds between
 each initialization, to avoid detection issues. Note that the second stage detects
 the 5th harmonic, the third stage detects the 7th harmonic and the 4th stage
 detects the 11th harmonic. An algorithm determines the two most predominant
 harmonics for compensation. Then, the two resonant controllers are dynamically
 340 tuned by the frequency feedback in accordance with the compensated harmonics.
 For example, between 2 seconds and 4 seconds, the 5th and 7th are the predominant
 harmonic components. From 4 seconds, the 7th and 11th harmonics are the
 predominant harmonic components.

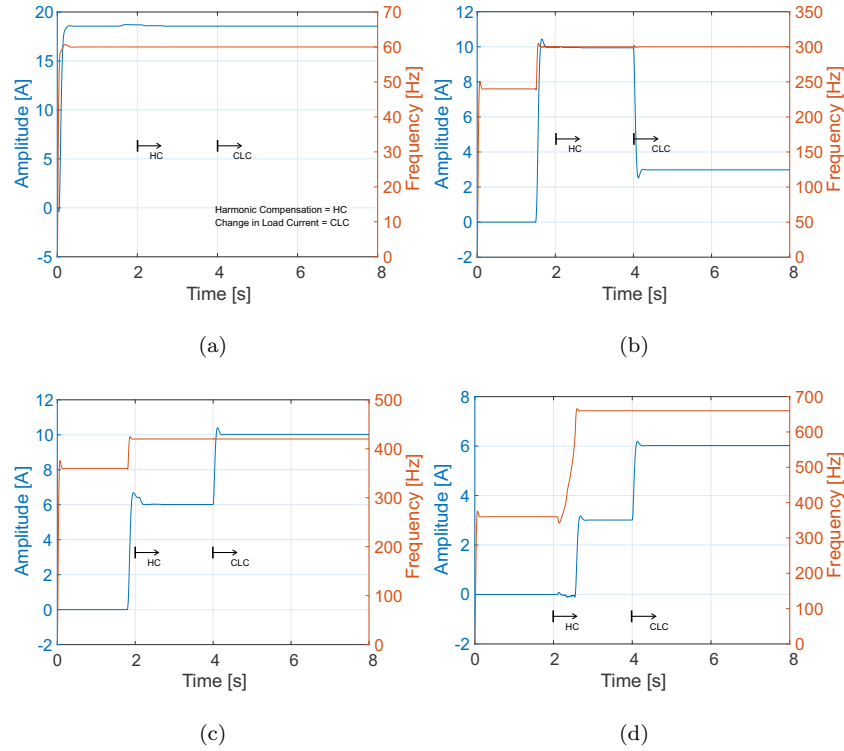


Figure 17: Amplitude and frequency detection dynamics of the load current (a) Load current fundamental component detection. (b) Harmonic detection of the 1st stage. (c) Harmonic detection of the 2nd stage. (d) Harmonic detection of the 4th stage.

Figure 18 shows inverter harmonic current components and Figure 19 shows grid harmonic current components. In $t < 1$ seconds, there is no compensation, and the grid current shows all the harmonics present in the system load. The grid current THD at this time is 126 %, as shown in Table 7. At $2 < t < 4$ seconds, the 5th and 7th harmonic components are compensated and appear in the inverter current. The grid current THD at this time is 32 %. In $t > 4$ seconds, the nonlinear load current changes, and the 7th and 11th harmonic components are compensated and the grid current THD remains as 32 %.

Similarly to the single-phase case study, it is made an analysis to verify the three-phase filter core and copper losses for currents of four harmonic

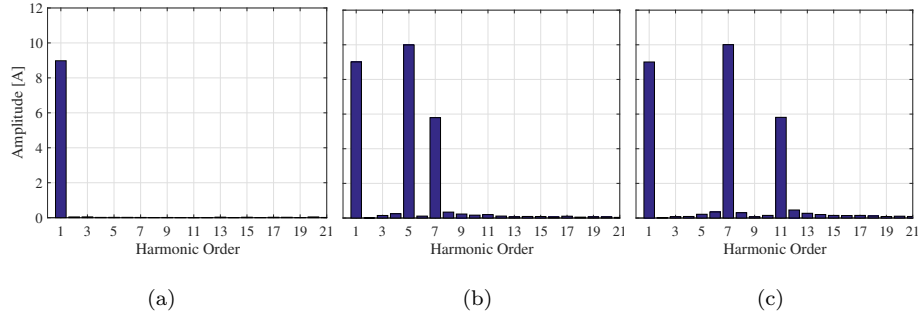


Figure 18: Inverter current spectra (a) without harmonic current compensation $t < 2s$, (b) compensating the first load profile $2 < t < 4s$ and (c) compensating the second load profile $t > 4s$

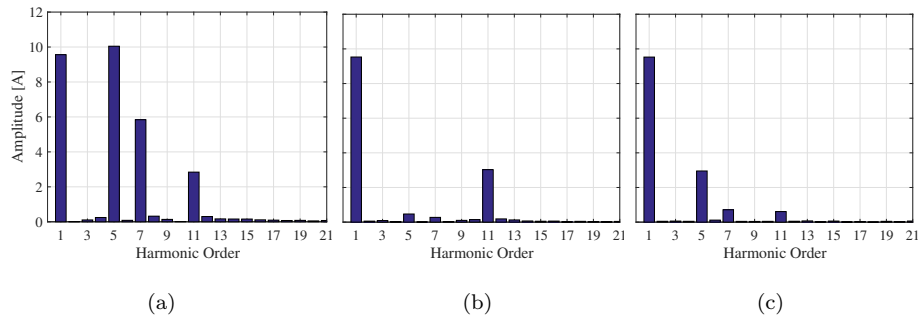


Figure 19: Grid current spectra (a) without harmonic current compensation $t < 2s$, (b) compensating the first load profile $2 < t < 4s$ and (c) compensating the second load profile $t > 4s$

Table 7: Grid current THD in the three-phase case study

Simulation Time (seconds)	Grid Current THD
$t < 2$	126 %
$2 \leq t < 4$	32 %
$t \geq 4$	32 %

orders, plus fundamental component, and five amplitude values. The system
 355 compensates the 5th, 7th, 11th and 13th harmonic current components, each one

with amplitude varying of 0.2 pu, 0.4 pu, 0.6 pu, 0.8 pu and 1 pu. Finally, the total losses, including three phases, are estimated. The obtained results are shown in Figure 20.

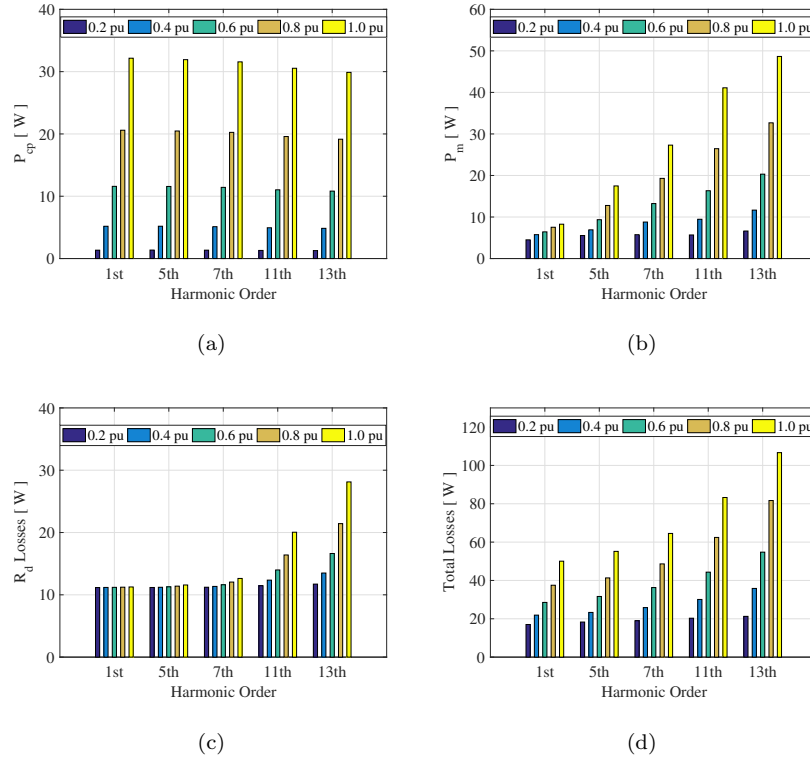


Figure 20: Losses in the three-phase LCL filter during harmonic compensation (a) Total copper losses (b) Total core losses (c) Damping resistor losses (e) Total LCL filter losses.

It is possible to note the same losses pattern shown and explained in Figure 15. Figure 20(a) shows the total inductor copper losses, including the three phases. For a same power and voltage, it is noted that the RMS value of the current in three-phase system is smaller than in the single-phase system, resulting in smaller copper losses. Figure 20(b) shows the total core losses, the core losses per inductor is similar in single and three-phase system.

Figure 20(c) shows the damping resistor losses. Although the RMS value

of the capacitor current decreases in the three-phase system in relation to the single-phase system, the sum of the damping resistor losses in the three phases is slightly greater than the losses in the single-phase damping resistor.

Finally, Figure 20(d) shows the total losses in the LCL filter. The LCL filter losses in the three-phase system are greater than in the single-phase system, due to losses in the inductor core and the damping resistor. When the PV system injects only the active power, the total losses are 50 W for 1 pu of fundamental current amplitude. Note that, when the PV inverter only injects 1 pu of 13th harmonic current, the total power losses are 106 W, approximately.

6. Conclusions

This work presents a detection and compensation method for harmonic load current components applied in single and three-phase PV inverters. The proposed method reduced the dominant harmonic current components, reducing significantly the grid current THD. The method presented good results for both single and three-phase converters.

Losses analysis showed that during harmonic current compensation, the LCL total losses is directly related with the harmonic order. Thus, the compensation of high order harmonic current components implies in higher losses. It is highlighted that the magnetic losses can increase almost four and five times during high order harmonic current compensation for single and three-phase systems, respectively. Moreover, the losses in the damping resistor is more than 20% of the total losses, thus, it is recommended other control strategies based on active damping techniques.

Therefore, the trade-off identified is the use of a PV inverter to reduce the grid current THD, increasing the inverter losses. Since harmonic current compensation is an ancillary service, it is recommended that the distribution network should to incentive the use of inverters with harmonic current compensation capacity, with focus to improve the overall power system.

7. Acknowledgments

395 This work has been supported by the Brazilian agencies CNPq (431478/2016–
3), FAPEMIG (*APQ* – 03555 – 16) and CAPES.

References

- [1] P. Rodriguez, A. Luna, I. Candela, R. Mujal, R. Teodorescu, F. Blaabjerg, Multiresonant frequency-locked loop for grid synchronization of power
400 converters under distorted grid conditions, *IEEE Trans. on Industrial Electronics*, 58 (2011) 127–138.
- [2] J. J. Conti, Annual Energy Outlook 2015 with projections to 2040, Technical Report, U.S. Energy Information Administration, 2015.
- [3] D. I. Brandão, F. P. Marafão, H. K. M. Paredes, A. Costabeber, Inverter
405 control strategy for DG systems based on the Conservative power theory, in: *IEEE Energy Conversion Congress and Exposition*, 2013, pp. 3283–3290.
- [4] M. Rekinge, F. Thies, G. Masson, S. Orlandi, Global Market Outlook:For Solar Power / 2015 - 2019, Technical Report, SolarPower Europe, 2014.
- [5] Y. Yang, F. Blaabjerg, H. Wang, Low voltage ride-through of single-phase
410 transformerless photovoltaic inverters, in: *IEEE Energy Conversion Congress and Exposition*, 2013, pp. 4762–4769.
- [6] J. He, Y. W. Li, F. Blaabjerg, X. Wang, Active harmonic filtering using current-controlled, grid-connected dg units with closed-loop power control, *IEEE Trans. on Power Electronics* 29 (2014) 642–653.
- 415 [7] L. S. Xavier, A. F. Cupertino, H. A. Pereira, Adaptive saturation scheme for a multifunctional single-phase photovoltaic inverter, in: *Int. Conf. on Ind. Appl.*, 2014, pp. 1–8.
- [8] J. P. Bonaldo, J. Antenor Pomilio, Multi-functional use of single-phase power converters, in: *IEEE PES Conf. on Innovative Smart Grid Technologies Latin America*, 2013, pp. 1–6.
420

- [9] J. P. Bonaldo, H. K. M. Paredes, J. A. Pomilio, Flexible operation of grid-tied single-phase power converter, in: Brazilian Power Electronics Conf., 2013, pp. 987–992.
- [10] H. A. Pereira, L. S. Xavier, A. F. Cupertino, V. F. Mendes, Single-phase
425 multifunctional inverter with dynamic saturation scheme for partial compensation of reactive power and harmonics keywords, European Conf. on Power Electronics and Applications (2015) 1–10.
- [11] H. Akagi, Y. Kanazawa, A. Nabae, Instantaneous Reactive Power Compensators Comprising Switching Devices without Energy Storage
430 Components, IEEE Trans. Ind. Appl. IA-20 (1984) 625–630.
- [12] Y. Yang, Advanced Control Strategies to Enable a More Wide-Scale Adoption of Single-Phase Photovoltaic Systems, Ph.D. thesis, Aalborg University, 2014.
- [13] IEEE Standard for Interconnecting Distributed Resources with Electric
435 Power Systems, IEEE Std 1547-2003 (2003) 1–28.
- [14] Photovoltaic (PV) systems - Characteristics of the utility interface, CEI/IEC Std 61727 - 2004 (2004) 1–23.
- [15] H. Fujita, H. Akagi, A practical approach to harmonic compensation in power systems-series connection of passive and active filters, IEEE Trans.
440 on Industry Applications 27 (1991) 1020–1025.
- [16] Y. Haiwen, G. Xin, M. Hanguang, Research on harmonic compensation effects for a kind of isolated power system, in: Int. Conf. on Electronic Measurement Instruments, 2009, pp. 4–686.
- [17] E. H. Watanabe, M. Aredes, Active and reactive instantaneous power
445 theory and applications - active filters and facts, Brazilian Congress of Automatic (1998) 81–122.

- [18] J. P. Bonaldo, H. K. M. Paredes, J. A. Pomilio, Control of single-phase power converters connected to low voltage distorted power systems with variable compensation objectives, *IEEE Trans. on Power Electronics* 31 (2016) 2039–2052.
- 450
- [19] B. P. McGrath, D. G. Holmes, J. J. H. Galloway, Power converter line synchronization using a discrete fourier transform (dft) based on a variable sample rate, *IEEE Trans. on Power Electronics* 20 (2005) 877–884.
- [20] Y. F. Wang, Y. W. Li, Three-phase cascaded delayed signal cancellation pll for fast selective harmonic detection, *IEEE Trans. on Industrial Electronics* 60 (2013) 1452–1463.
- 455
- [21] W. Yanfeng, S. Rongyan, G. Xinhua, L. Yan, Y. Hua, The comparative analysis of pi controller with pr controller for the single-phase 4-quadrant rectifier, in: *Conf. and Expo Transp. Electrifi. Asia-Pacific*, 2014, pp. 1–5.
- [22] L. S. Xavier, A. F. Cupertino, V. F. Mendes, H. A. Pereira, A novel adaptive current harmonic control strategy applied in multifunctional single-phase solar inverters, in: *Braz. Power Elec. Conf.*, 2015, pp. 1–6.
- 460
- [23] M. Ciobotaru, R. Teodorescu, F. Blaabjerg, A new single-phase pll structure based on second order generalized integrator, in: *IEEE Power Electronics Specialists Conf.*, 2006, pp. 1–6.
- 465
- [24] M. G. Villalva, J. R. Gazoli, E. R. Filho, Comprehensive approach to modeling and simulation of photovoltaic arrays, *IEEE Trans. Power Electron.* 24 (2009) 1198–1208.
- [25] D. Sera, L. Mathe, T. Kerekes, S. V. Spataru, R. Teodorescu, On the perturb-and-observe and incremental conductance mppt methods for pv systems, *IEEE Journal of Photovoltaics* 3 (2013) 1070–1078.
- 470
- [26] M. Liserre, F. Blaabjerg, S. Hansen, Design and control of an lcl-filter-based three-phase active rectifier, *IEEE Trans. on Ind. Appl.* 41 (2005) 1281–1291.

- [27] V. Kaura, V. Blasko, Operation of a phase locked loop system under
475 distorted utility conditions, *IEEE Trans. on Ind. Appl.* 33 (1997) 58–63.
- [28] A. P. L. Cota, R. C. Abrantes, P. C. Cortizo, R. A. S. Santana, W. C. Padro,
Comparison of three 3-phase converter topologies for ups applications, in:
Brazilian Power Electronics Conf., 2015, pp. 1–6.
- [29] Powder Cores, Magnetics International Pittsburg P A Catalog, 2006.
- 480 [30] J. Mhlethaler, J. W. Kolar, A. Ecklebe, Loss modeling of inductive
components employed in power electronic systems, in: *Int. Conf. on Power
Electronics*, 2011, pp. 945–952.
- [31] F. Blaabjerg, R. Teodorescu, M. Liserre, A. V. Timbus, Overview of control
and grid synchronization for distributed power generation systems, *IEEE*
485 *Trans. on Industrial Electronics* 53 (2006) 1398–1409.
- [32] M. G. Villalva, T. G. D. Siqueira, E. Ruppert, Voltage regulation of
photovoltaic arrays: small-signal analysis and control design, *IET Power
Electronics* 3 (2010) 869–880.
- 490 [33] A. G. Yepes, F. D. Freijedo, O. Lopez, J. Doval-Gandoy, Analysis and
Design of Resonant Current Controllers for Voltage-Source Converters by
Means of Nyquist Diagrams and Sensitivity Function, *IEEE Trans. on
Industrial Electronics* 58 (2011) 5231–5250.